Received: 29 January 2021 | Revised: 28 September 2021 | Accepted: 2 October 2021

DOI: 10.1002/eqe.3562

RESEARCH ARTICLE

WILEY

A simplified approach for including the incidence angle effect in seismic risk assessment

Yeudy Felipe Vargas-Alzate[1] | **Vitor Silva**[2,3] | **Dimitrios Vamvatsikos**[4] | **Lluis Gonzaga Pujades**[1]

[1] Departament d'Enginyeria Civil i Ambiental, Universitat Politècnica de Catalunya · BarcelonaTech (UPC), Barcelona, Spain

[2] Global Earthquake Model Foundation, Pavia, Italy

[3] Faculty of Science and Technology, University Fernando Pessoa, Porto, Portugal

[4] School of Civil Engineering, National Technical University of Athens, Athens, Greece

Correspondence
Yeudy Felipe Vargas-Alzate, Universidad Politécnica de Cataluña, Barcelona, Spain.
Email: yeudy.felipe.vargas@upc.edu

Funding information
This project has received funding from the European Union's Horizon 2020 research and innovation programme under the Marie Skłodowska-Curie grant agreement No 799553

Abstract

A simplified procedure is developed to consider the azimuthal orientation of buildings when estimating seismic risk. Two square-plan reinforced concrete building models are considered as a testbed, one with similar and one with dissimilar properties along the two principal horizontal axes. The fragility of both structures is analysed using a set of ground motion records rotated to multiple incidence angles to develop orientation-dependent fragility functions. It has been observed that, re-orienting all records so that these structures have the same azimuth vis-à-vis the corresponding epicentre leads to significant differences compared to assuming random orientations. Additional results stemming from single-degree-of-freedom oscillators further confirm such findings, showing a dependence to the proximity to the faults and the level of dissimilarity in the principal horizontal axes of the structure. The end results point to a non-negligible bias in assessment studies when a structure's orientation with respect to governing rupture scenarios is not taken into account. It is shown that the median of fragility curves calculated for un-rotated incidence angles can be bias-corrected through shifted by an amount that depends on the azimuthal orientation and level of axes-dissimilarity of structures.

KEYWORDS
directionality effect, cloud analysis, consistent rotations, seismic risk assessment

1 | INTRODUCTION

Seismic risk assessment is characterized by a wide range of epistemic and aleatory sources of uncertainty.[1] They lead to a high variability on the estimated structural damage due to an earthquake. For instance, reconnaissance reports from past events have highlighted situations in which nearby structures shared similar typological characteristics, yet very different damage levels.[2,3] Amongst many others, such variations may be explained by the randomness associated to the mechanical properties of the materials, structural interventions, variability in the soil conditions, or the different orientation of similar buildings vis-à-vis incoming seismic waves. The latter aspect is commonly known as the directionality effect, and there is evidence that it is a fairly strong aspect of ground motions recorded in short to moderate distances from the rupture (e.g., see[4] on the 2010–2011 Canterbury events).

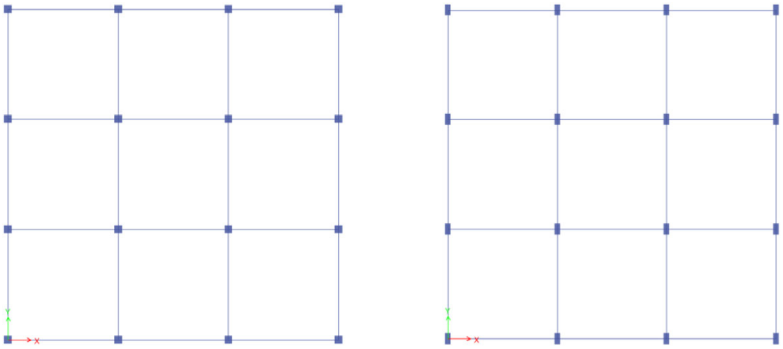

FIGURE 1 Plan view of the first floor for the similar-axes (Left) and dissimilar-axes (Right) buildings

The azimuthal angle of seismographs is commonly oriented to coincide with the North-South and East-West global directions. It implies that a recorded signal is unlikely to contain, at least explicitly, the maximum intensity that occurs at the seismic station. Several strategies to identify in which direction this intensity occurs at the ground level can be found in.[5] Other researchers have oriented their efforts towards finding the direction of the maximum acceleration in the response of single-degree-of-freedom (SDoF) oscillators.[6] They have found that this direction as well as the amount of variability due to the incidence angle are functions of the fundamental period of the analysed system. This indicates that within an urban environment stricken by an earthquake, similar structures may suffer different damage due to the incidence angle of the seismic waves. The influence of this angle on the structural response has been widely studied.[7–11] In general, they have found that the seismic response of a structure significantly varies depending on the incidence angle.

Regarding the influence of the incidence angle in seismic risk estimations, Lagaros[12] presented the multicomponent incremental dynamic analysis, which incorporates the record-to-record variability and the one related to the incidence angle. Torbol and Shinozuka[13] proposed introducing the directionality effect in the assessment of lifeline systems, at the cost of requiring computer-intensive calculations of fragility at different incidence angles. Vargas-Alzate et al.[14] have studied the seismic response of a population of very similar buildings, which were located close to each other, that exhibited very different damage levels despite being subjected to the same ground motion. They have shown that when the record-to-record variability can be omitted (because the ground motion is known), the ones related to the mechanical properties of the structure and the incidence angle may explain the discrepancies of the observed damage. Pinzón et al.[15] also studied the variability of the damage caused by the *19 September 2017 Mw 7.1 central Mexico earthquake* to a group of very similar adjacent buildings. They traced the direction followed by seismic waves maximizing the acceleration response of an SDoF system considering the ground motion records provided by the closest seismic stations. They have found that the horizontal direction in which the maximum spectral acceleration at the fundamental period of the structure occurred coincided with the most flexible axis of a collapsed building in the group. Despite such evidence, the incidence angle effect is not systematically considered in estimates of seismic risk. It has been argued that when the orientation of a structure's principal axes relative to the seismic rupture is unknown, e.g., due to limited information on the building, or high variability of the location of the rupture itself, it is computationally more efficient to only consider a single random orientation per ground motion record employed.[16,17] This article is aimed at developing a simplified procedure to account for the effect of directionality by offering a baseline approach for bias-correcting fragility functions of structures.

2 | BUILDING MODELS

Two square-plan reinforced concrete buildings are considered as a testbed. Their structural properties represent buildings located in low-to-moderate seismic environments. It means that capacity-design rules have not been implemented in the modelling process. The first building, termed 'similar-axes', has square columns and is completely symmetric, having the same strength, stiffness and mass properties in both of its principal axes; the second has rectangular columns, thus becoming stiffer in one axis versus the other. Henceforth it will be referred to as the 'dissimilar-axes' building. Figure 1 (Left) shows a plan view of the first floor of the similar-axes building model. It has four storeys of 3 m height and three spans in each direction of 5 m length. The fundamental periods in the main directions, T_X and T_Y, are both 0.657 s. Since the columns are oriented so that their sides are orthogonal to the main axes, the horizontal stiffness is higher for any other direction than these ones. Due to the rotational symmetry, the response of this building to different incident angles has a periodicity of 90°.

TABLE 1 Geometrical properties; 'h' indicates the height while 'w' the width of the element; subscripts 'c' and 'b' denote column and beam, respectively; ρ_c and ρ_b are the steel percentages for columns and beams, respectively

	Similar-axes building						Dissimilar-axes building					
	h_c (m)	w_c (m)	ρ_c (%)	h_b (m)	w_b (m)	ρ_b (%)	h_c (m)	w_c (m)	ρ_c (%)	h_b (m)	w_b (m)	ρ_b (%)
Story 1	0.35	0.35	1	0.30	0.35	0.66	0.50	0.25	1	0.30	0.35	0.66
Story 2	0.35	0.35	1	0.30	0.35	0.66	0.50	0.25	1	0.30	0.35	0.66
Story 3	0.30	0.30	1	0.30	0.35	0.66	0.35	0.25	1	0.30	0.35	0.66
Story 4	0.30	0.30	1	0.30	0.35	0.66	0.35	0.25	1	0.30	0.35	0.66

As commented above, the dissimilar-axes building model is created by replacing the square shape of the columns of the similar-axes building by rectangular ones of the same reinforcement and practically the same area, without changing the beams, maintaining practically the same capacity to vertical loads as in the first building. As a consequence of this modifcation, the periodicity of the horizontal response is 180°. Figure 1 (Right) shows a plan view of the first floor of this building. The fundamental periods in the principal directions, T_X and T_Y, are 0.745 s and 0.586 s, respectively. This way, one would expect this structure to suffer higher deformations when the direction of the most energetic seismic waves is parallel to the x-axis. Table 1 presents the geometric properties of the structural elements comprising both models.

The axis-dissimilarity of the structures can be characterized by the ratio of the highest to the lowest fundamental period in the principal directions ($R_{T_{XY}}$, see Eq. 1). Accordingly, $R_{T_{XY}} = 1$ for the similar-axes structure and $R_{T_{XY}} = 1.2713$ for the dissimilar-axes one.

$$R_{T_{XY}} = \frac{T_X}{T_Y} \tag{1}$$

The modified Takeda hysteresis law[18] has been used to represent the in-cycle behaviour of the structural elements (beams and columns). This law allows considering strength degradation due to large deformations and excessive number of inelastic cycles. To do so, a strength degradation function, which depends on the ductility reached by the structural elements as well as a degrading coefficient associated to the number of inelastic cycles has been considered in the hysteretic model.[19] A hardening coefficient equal to 5% has been considered for the post-yielding branch of the elements. For the stiffness degradation, the α degrading factor has been fixed to 0.4. The yielding surfaces are defined by the bending moment-axial load interaction diagram for columns and bending moment-curvature for beams. P-Delta effects and the large-displacement theory have been considered in the numerical model, as the structures analysed may experience deformations beyond the elastic range, sometimes even exceeding their capacity to withstand gravity loads. The elastic modulus and the concrete compressive strength have been set to 23 GPa and 25 MPa, respectively. For the steel reinforcement, the elastic modulus and the yielding limit have been set to 219 GPa and 460 MPa, respectively. Dead and Live loads are 4 kPa and 1 kPa, respectively. The steel percentage for columns, ρ_c, have been considered equal to 1%, whilst for beams, ρ_b, this value has been set at 0.66%.

In accordance with the above, the capacity curves in the main directions of both structures have been calculated. Figure 2 shows one capacity curve for the similar-axes structure and two for the dissimilar-axes one. These curves reflect the high dependence of the horizontal capacity of the buildings against the variation of the size of their structural elements. This has important consequences in estimating seismic risk, as will be shown later in this article.

3 | RECORD SELECTION

There are several methodologies to select ground motion records.[20] Typically, the goal is to have sufficient records that lead the structure to different performance levels. However, the availability of strong earthquake records with high values of the conditioning intensity measure (IM) is a common restriction found in current databases. This triggers excessive scaling of ground motion records that can introduce bias in the structural response.[21] In order to mitigate such issues when employing cloud analysis,[22] the following procedure has been used for selecting and scaling (where necessary) one-hundred ground motion records:

1. Selection of the database
2. Identification of the IM
3. For each record of the database, calculation of the identified IM
4. Definition of IM intervals; in this study ten increasing intervals have been considered

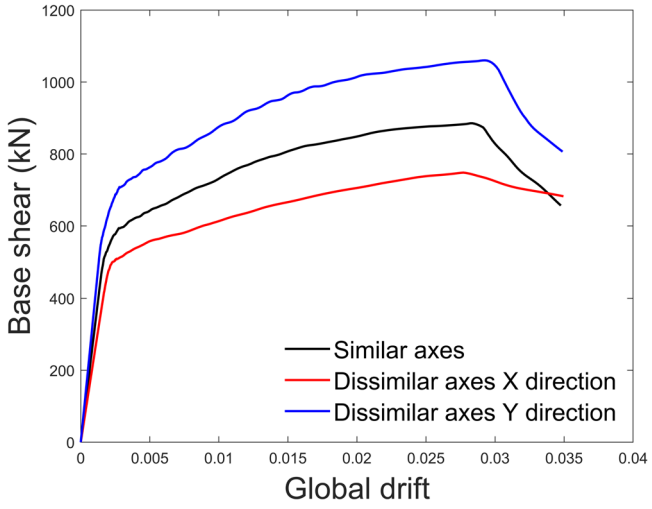

FIGURE 2 Capacity curves of the similar- and dissimilar-axes buildings

5. Per each interval, selection of ten records whose IM value belongs to the interval
6. If an interval does not contain enough records, an appropriate number of them is selected and scaled from the previous interval; this criterion is meant to avoid excessive scaling of the ground motion records

The engineering strong motion database of Luzi et al.[23] has been adopted. Identifying the IM (step 2) to properly select ground motion records mainly depends on its efficiency and sufficiency.[24] An efficient IM has low conditional response variability, while a sufficient one renders the conditional response distribution independent of other ground motion characteristics. The spectral acceleration at the fundamental period, $\mathrm{Sa}(\mathrm{T}_1)$, is one of the most used IMs. However, unless hazard-consistent record selection is employed,[25] it has been shown to introduce bias when scaling. Instead, an IM based on the geometric mean of spectral acceleration values estimated at periods covering both higher and elongated modes of response, Sa_{avg}, is more efficient and sufficient than $\mathrm{Sa}(\mathrm{T}_1)$.[26–28] Analogous to this concept, an IM identified as AvSa is considered herein to perform the analysis. AvSa differs from Sa_{avg} since it is calculated using the arithmetic instead of the geometric mean. As 3-D structural analyses are performed, the IM should also consider the fundamental periods of the structure in both main directions. To do so, the average of the fundamental periods in each direction, T_{XY}, is used to define the period interval for calculating AvSa. It is worth noting that AvSa varies due to the rotation of the horizontal components of the ground motion records. For the sake of simplicity, this IM has been estimated from the un-rotated (UR) components. Moreover, AvSa values are chosen to be almost uniformly distributed along the interval (Steps 5 and 6).

As commented above, the interval around T_{XY} should consider softening of the structure due to the accumulation of damage and the participation of higher modes. Vargas-Alzate et al.[29] have found that using $0.1T_1$ and $1.8T_1$ as limits minimizes the mean square error between engineering demand parameter (EDP) values estimated via nonlinear dynamic analysis (NLDA) and a modified version of the equal displacement rule. Since these limits were calculated for buildings in the range of periods 0.4-1 s, they are employed herein. Figure 3 (Top, left) shows an example of the calculation of AvSa for a single ground motion record.

Figure 3 (Top, right) shows the evolution of AvSa as a function of the incidence angle θ. Notice that T_{XY} is similar in both structures; for the similar-axes structure, T_{XY} is equal to 0.657 s whilst for the dissimilar one it is equal to 0.665 s. According to this, the same set of earthquake records is used for both structures. The intensity levels defining the upper and lower limits of each stripe (step 4) range from 0 to 0.6 g at intervals of 0.06 g. In total, 92 records were directly selected from the strong motion database, and only 8 records were scaled to fill in deficient intervals. Figure 3 (Bottom) shows the geometric mean spectra of the selected records.

4 | DERIVATION OF FRAGILITY FUNCTIONS

Using the one-hundred UR signals selected, NLDAs are performed for both buildings. As an EDP it is employed the maximum inter-storey drift ratio, MIDR, which characterizes structural and non-structural drift-sensitive damage.[1] While

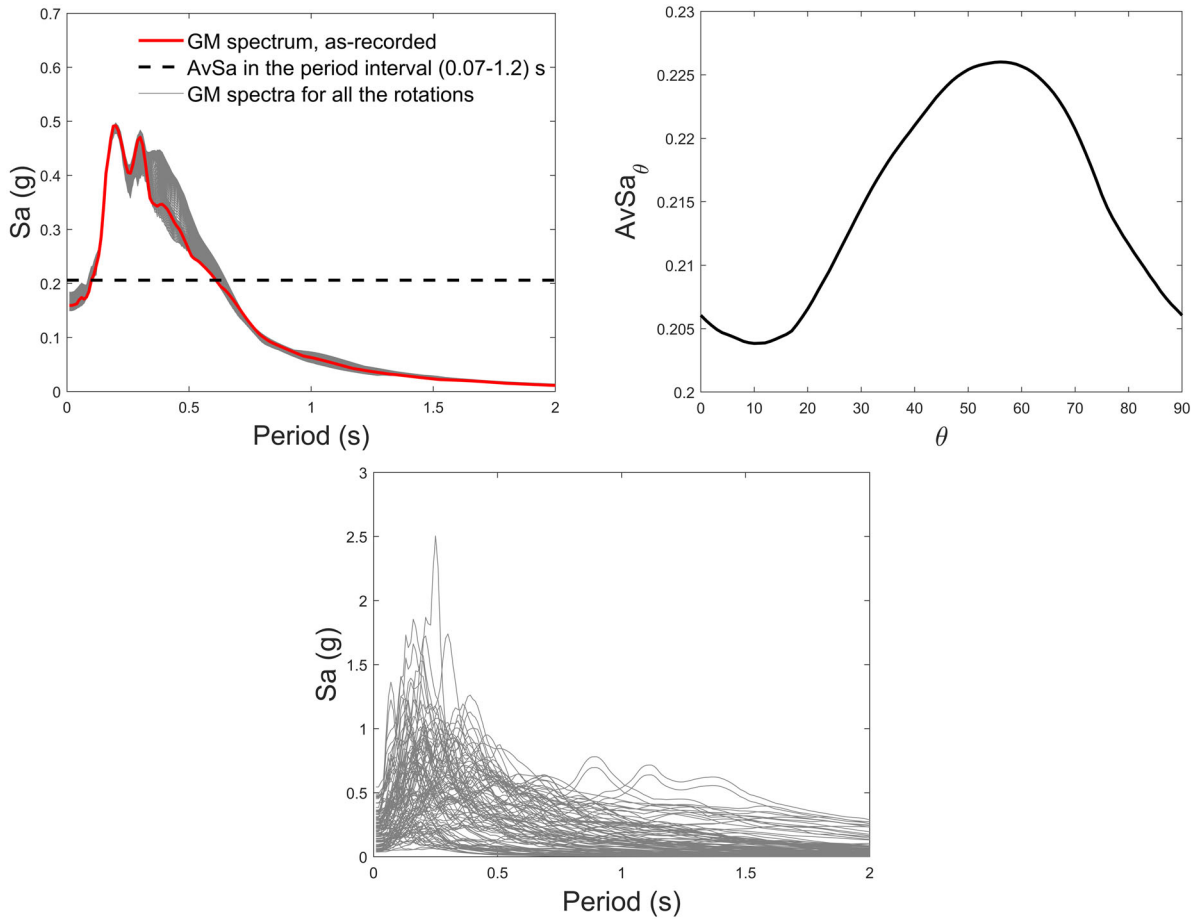

FIGURE 3 Top, left: GM spectra variability due to the incidence angle. Top, right: Evolution of AvSa as a function of the incidence angle. Bottom: GM spectra of the selected ground motion records

it is common practice to employ the MIDR of the two main axes separately, it has been chosen to use instead their SRSS value. This is less variable than the individual axes MIDR values and it helps increase the statistical significance of the results for the given number of records. In other words, it will help to better discern the trends from the noise, but at the same time it will lower the apparent difference between the cases studied. Thus, for a storey i, the evolution of the inter-storey drift in the n direction, $IDR_{i,n}(t)$, is given by:

$$IDR_{i,n}\ (t) = \frac{\delta_{i,n}\,(t) - \delta_{i-1,n}\,(t)}{h_i} \tag{2}$$

where $\delta_{i,n}(t)$ is the displacement at the floor i of the structure in the n direction; h_i represents the height of the storey i. The maximum inter-storey drift ratio at the storey i, $\mathrm{MIDR_i}$, can be calculated as follows:

$$\mathrm{MIDR_i} = max\left(\sqrt{IDR_{i,x}^2\,(t) + IDR_{i,y}^2\,(t)}\right) \tag{3}$$

The maximum inter-storey drift ratio observed in the building, MIDR, is given by:

$$\mathrm{MIDR}\ = max\left[\mathrm{MIDR_1}, \mathrm{MIDR_2} \ldots \mathrm{MIDR_{N_{st}}}\right] \tag{4}$$

where $\mathrm{N_{st}}$ represents the number of stories of the building. Figure 4 (Top, left) shows one-hundred IM-EDP pairs obtained per each structure. It can be seen that the dissimilar-axes structure presents a slightly higher response than the similar-axes one. In addition, there is one point per structure where collapse has occurred, as the MIDR clearly exceeds the deformation capacity of the structure of about 3% (see Figure 2). If significantly more collapsing runs were present, one would have to adopt a separate characterization of collapse and non-collapse results.[30] Since only one such case is present per structure,

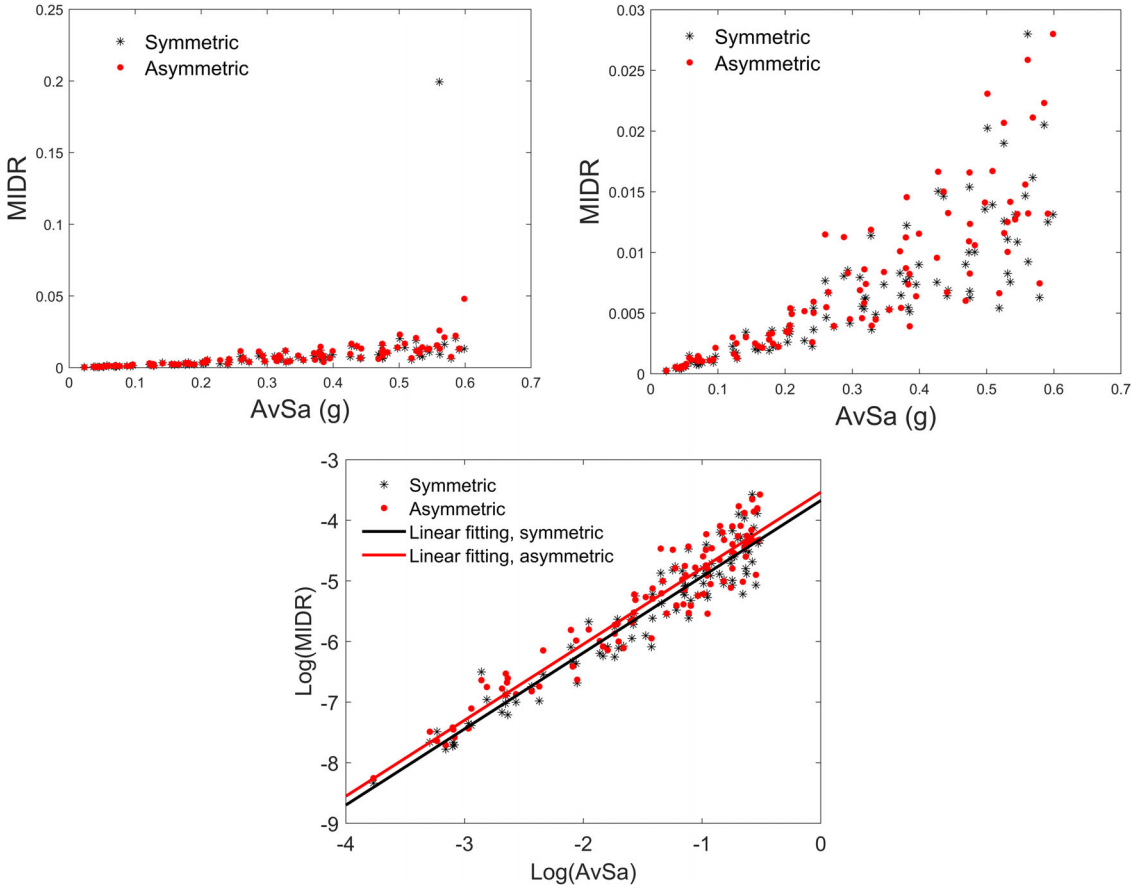

FIGURE 4 Top, left: MIDR computed from the NLDA. Top, right: MIDR exceeding 0.028 have been set to this value for display purposes. Bottom: IM-EDP pairs in the log-log space

it has been opted to neglect this in subsequent calculations and only visualize the corresponding MIDRs by setting it at a maximum value of 2.8% (Figure 4, top, right).

Following the cloud analysis approach, linear regression is performed in the log-log space (see Figure 4, bottom). The resultant line is used to estimate the expected value of a parametric statistical distribution given an IM value. The variability of this parametric distribution is calculated as the standard deviation of the IM-EDP residuals with respect to the fitted line. Then, specific drift capacity values, $MIDR_C$, can be used to establish performance thresholds describing the expected damage of buildings, if exceeded. The evolution of the probability of exceeding one of these thresholds given the IM value is known as an analytical fragility function, e.g.[31] A simplified approach to derive these curves based on the capacity spectrum method (CSM) obtaining similar results to those based on the comprehensive NLDA can be found in Vargas-Alzate et al.[32]

In the present study, $MIDR_C$ thresholds have been defined taking into account the damage index (DI) of Park and Ang.[33] This index provides a quantification of the expected seismic damage depending on the maximum ductility reached by the structural elements as well as the energy dissipated. Figure 5 shows the relationship between DI and MIDR for both structures. From a polynomial regression analysis, the mean curve relating DI and MIDR is estimated. This curve is used to obtain $MIDR_C$ thresholds (see Figure 5) according to the DI intervals considered in,[34] corresponding to the damage states of none, slight, moderate, extensive and complete, as well as a (nominal) collapse state.

Once the damage states and their respective thresholds have been defined, the fragility functions can be derived. Figure 6 shows the results for both structures (Left and right for the similar- and dissimilar-axes, respectively).

Having enough IM-EDP pairs is paramount in deriving unbiased fragility functions according to the selection criteria of the ground motions (see Section 3). To achieve this, the optimal number of pairs can be estimated by analysing the evolution of the parameters involved in the calculation of fragility functions, when the number of records increases. These parameters are the vertical intercept, the slope of the regression line, and the standard deviation of the residuals (see Figure 7). In other words, the objective is to find the number of records which stabilizes the above-mentioned parameters.

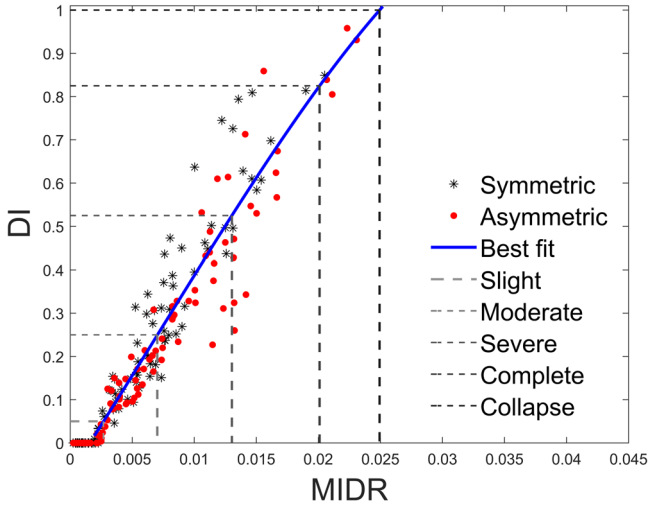

FIGURE 5 Damage threshold definition according to the damage index of Park and Ang[33]

TABLE 2 Damage thresholds definition

Damage state	DI	$MIDR_C$
Slight (Sl)	0.050	0.0027
Moderate (Mo)	0.250	0.0070
Extensive (Ex)	0.525	0.0130
Complete (Cm)	0.825	0.0200
Collapse (Cl)	1.000	0.0250

It can be seen that from sixty records onwards, the curves stabilize for vertical intercept and the slope of the regression curve (see Figure 7, top). For the standard deviation of the residuals (Figure 7, bottom), it is observed that from eighty records onwards this variable tends to be stable. However, it has been preferred to use the entire set of records to derive fragility functions.

It is worth mentioning that the number of records per interval to estimate the parameters shown in Figure 7 is constant. It means, for instance, that results for ten records are obtained by considering one record per interval, for twenty, two records per interval, and so on.

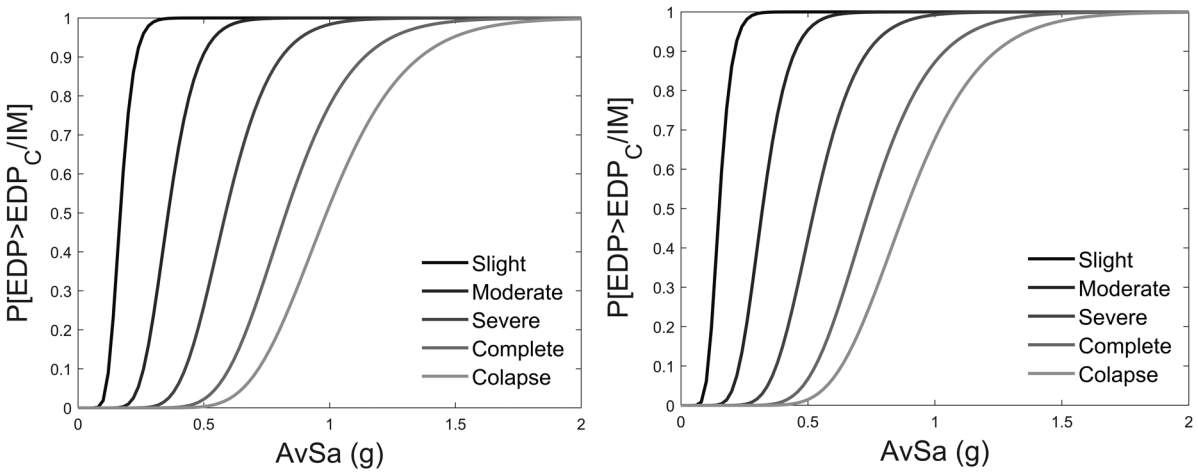

FIGURE 6 Fragility functions for several damage states. Left: Similar-axes structure. Right: Dissimilar-axes structure

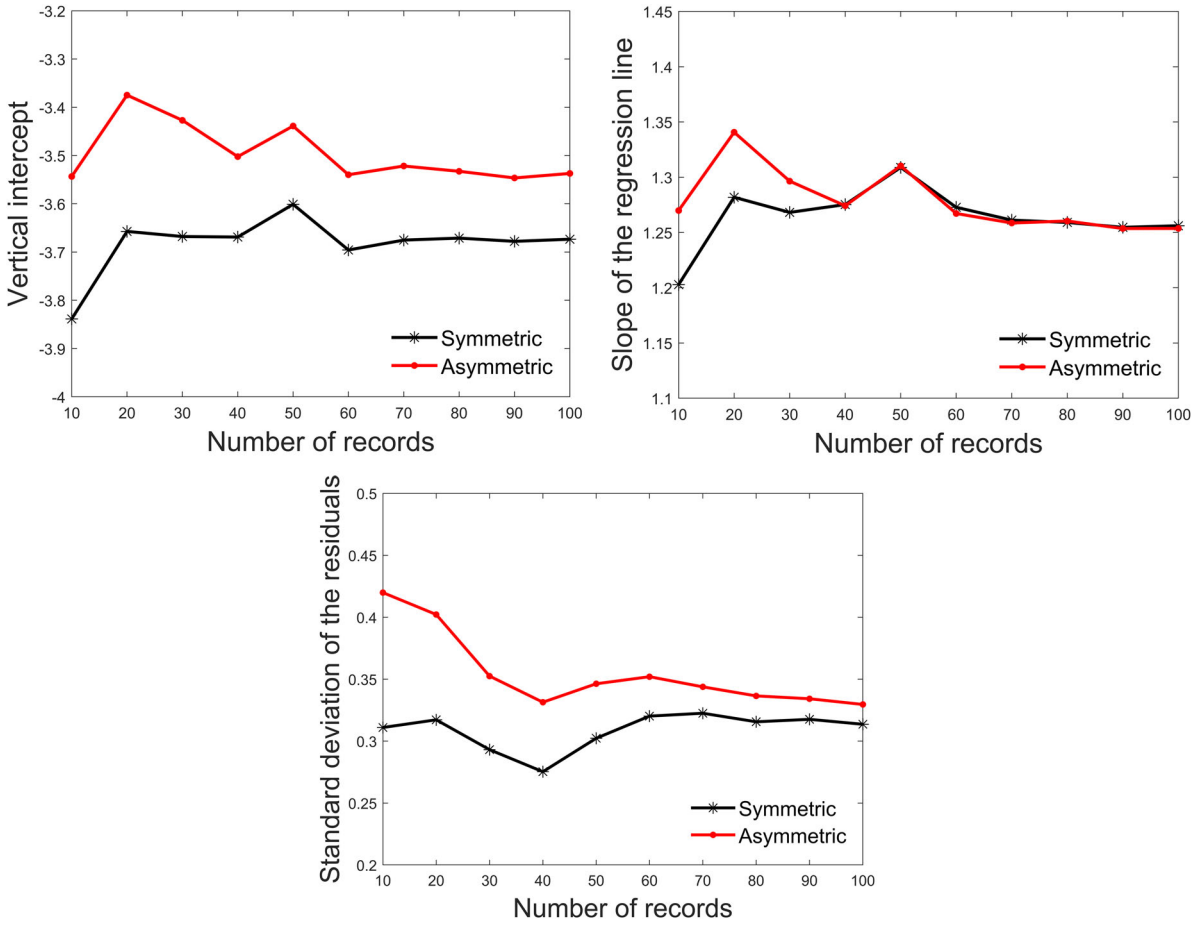

FIGURE 7 Evolution of the vertical intercept (Top, left), slope (Top, right), and standard deviation of the residuals (Bottom) of the IM-EDP pairs as a function of the number of records

5 | VARIABILITY IN THE FRAGILITY FUNCTIONS DUE TO THE INCIDENCE ANGLE

The fragility functions presented in Figure 6 are calculated by assuming that the main axes of both structures are parallel and orthogonal to the North-South and East-West global directions. However, the azimuthal orientation of actual buildings in urban environments mainly depends on the disposition of the grid of main streets. One may opt to call it uncertain, or take it into account. For the latter, a first step should be to quantify how much a fragility function may vary if a rotation of the set of records is performed.

5.1 | Structural response as a function of the incidence angle

To quantify the influence of the incidence angle on the structural response, the set of ground motion records is rotated to calculate new MIDR values. Because of the different rotational symmetry of the structures, the horizontal components of the records have been rotated from 0° to 90° for the similar-axes structure, and from 0° to 180° for the dissimilar one; in both cases increments of 1° are considered. Figure 8 (Left) presents the variation of the MIDR as a function of the incidence angle for the similar-axes structure. This figure shows that the nonlinear dynamic response of a building close to collapsing is highly variable; note that one record triggers the collapse of the structure if it is rotated at certain angles. One could attribute this high variability to numerical errors in the software. However, it has been observed that the most erratic responses are related to records whose spectra are very sensitive to rotations. Since only one signal displays such extreme variability, it has been excluded from further processing when excessively exceeding the collapse MIDR threshold, without biasing the statistics. In Figure 8 (Right), the rotational response of the structure to a specific record has been highlighted (Red line). It is possible to observe that some angles caused the structure to reach thresholds related

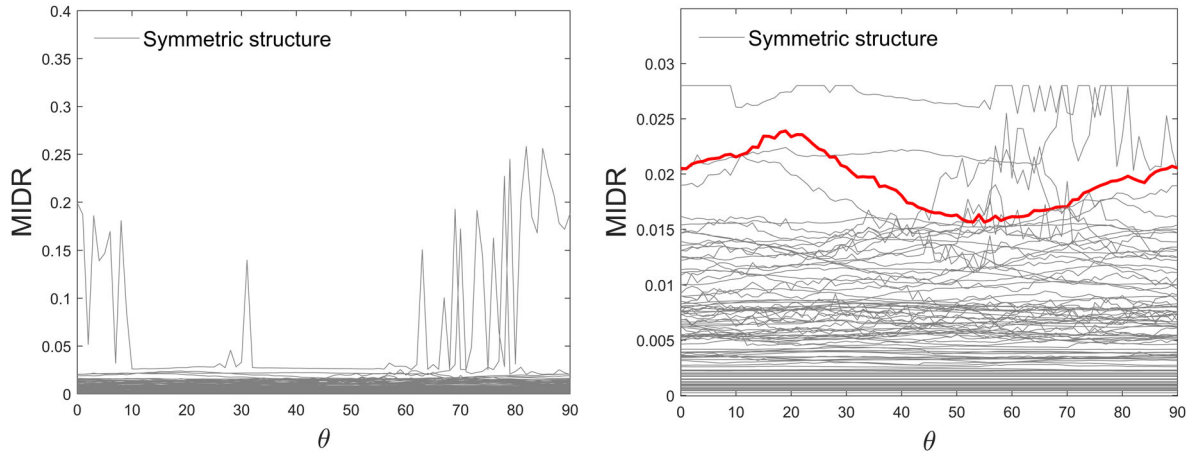

FIGURE 8 MIDR variability due to the incidence angle for the similar-axes structure. Left: MIDRs computed from the NLDA. Right: MIDRs exceeding 0.028 have been set to this value for display purposes; the red line is related to a ground motion record that makes the structural response very sensitive to variations in the incidence angle

to complete damage state (from 0° to 30°); if the same record is rotated to angles varying from 30° to 85°, extensive damage is reached. Such variations may partially explain differences of the observed damage in similar structures subjected to the same record, but having different azimuthal orientations. Of course, these variations can also come from other sources of uncertainty, e.g. mechanical properties, local soil conditions, etc.

Figure 9 (Left) shows the variation of the MIDR as a function of the incidence angle for the dissimilar-axes structure. It can be seen that the rotational response of this structure is much more erratic than the similar-axes one. The number of collapses increased when compared to the similar-axes structure. Now up to three records may cause collapse in some incidence angle scenario, and being few enough were treated similarly as in previous cases. It has been verified that less than 16% of the records were excluded per intensity bracket.[35] Figure 9 (Right) highlights the results provided by a ground motion producing high variability in the response. The variation observed indicates that, for a rotation of around 42°, the building is very close to collapsing; for an angle around 140°, only moderate damage is expected.

Figures 10 (Top, left and right) show the IM-EDP pairs for both structures, using as IM their values at the original UR axes. It is important to note that the variability due to the incidence angle increases along with the intensity. In spite of this, if fragility functions are calculated using all the IM-EDP pairs, one would obtain almost exactly the same results as using the UR signals. This does not mean that the influence of the incidence angle is negligible, but that it fades when considered simultaneously with the record-to-record variability.[16]

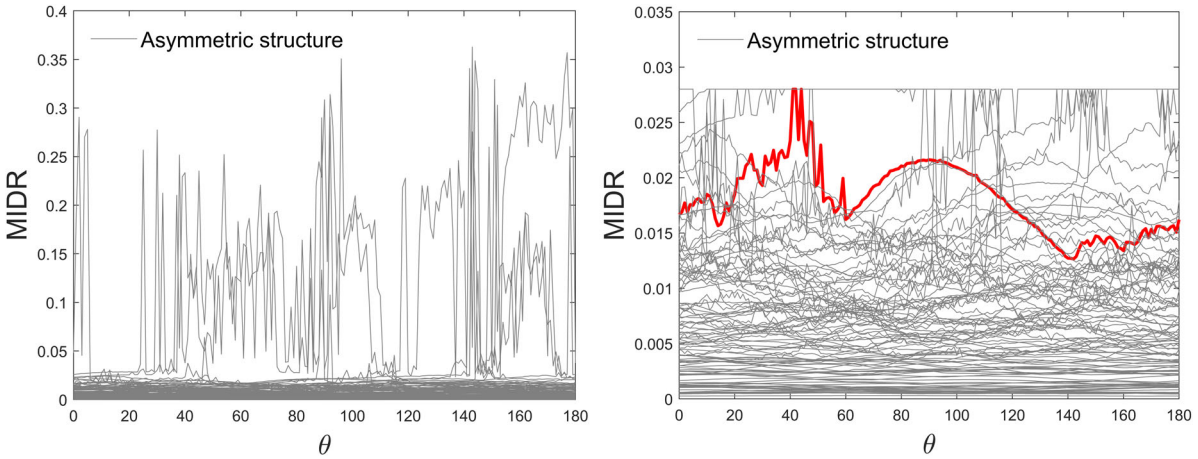

FIGURE 9 MIDR variability due to the incidence angle for the dissimilar-axes structure. Left: MIDRs computed from the NLDA. Right: MIDRs exceeding 0.028 have been set to this value for display purposes; the red line is related to a ground motion record that makes the structural response very sensitive to variations in the incidence angle

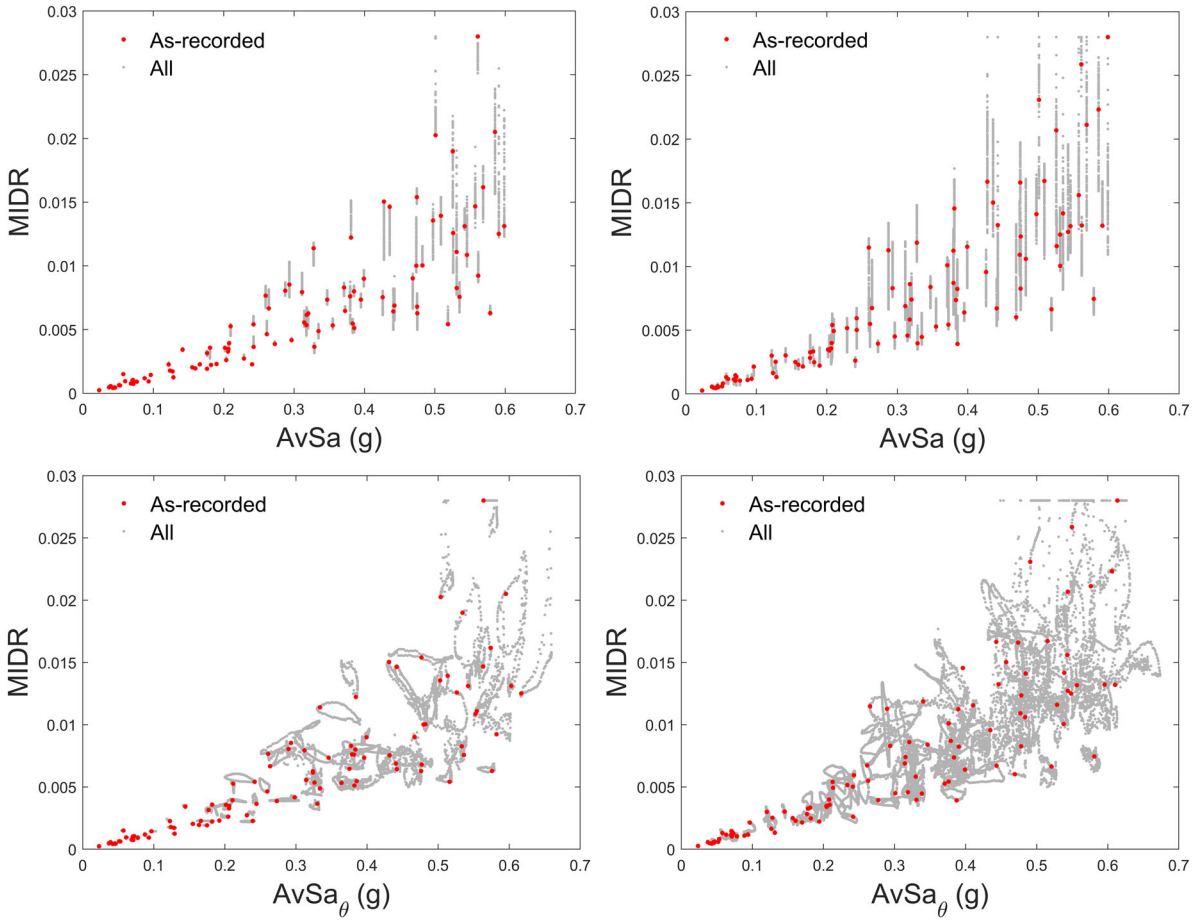

FIGURE 10 Top: MIDR as a function of the IM. Bottom: MIDR considering the variability of the IM given the incidence angle. Left: Similar-axes structure; Right: Dissimilar-axes structure

In Figure 3 (Top, right), one can see that AvSa varies when rotating the signal; if this variability were considered (i.e. using the IM-EDP pairs coming from Figures 10, bottom, left and right), the standard error related to the regression analysis of IM-EDP pairs increases around 12% with respect to that in which the IM does not vary (i.e. Figures 10, top, left and right). It has been opted not to include this variability in the analysis since ground motion prediction equations are nowadays derived for direction-independent IMs.[6]

In order to show how the axes dissimilarity in a structure may affect its potential risk, Figure 11 displays a histogram containing the ratios between the highest and the lowest MIDR, for the analysed ground motion records. It can be seen that these statistical distributions are considerably different. For instance, the median ratio in the similar-axes structure is located at 1.19, whilst for the dissimilar-axes one it lies at 1.63. This demonstrates that the variability in the response due to the incidence angle is much higher if the main axes present different properties.

5.2 | Incidence-agnostic fragility functions

Incidence-agnostic fragility functions are those that have not been developed for any consistent rotation of the ground motion record with respect to the location of both rupture and structure. These fragility functions reflect the inherent variability associated to the randomness of the incidence angle of the ground motion records and the azimuthal position of a structure.

Incidence-agnostic fragility functions have been calculated with the MIDR values obtained for each of the incidence angles considered above. This is equivalent to assuming that the buildings are rotated clock-wise starting from the un-rotated components, i.e. $\theta = 0°$, up to 90° for the similar-axes structure, and up to 180° for the dissimilar one. In this way, Figure 12 (Top, Left) shows 90 fragility functions calculated for the similar-axes structure and 180 for the dissimilar one

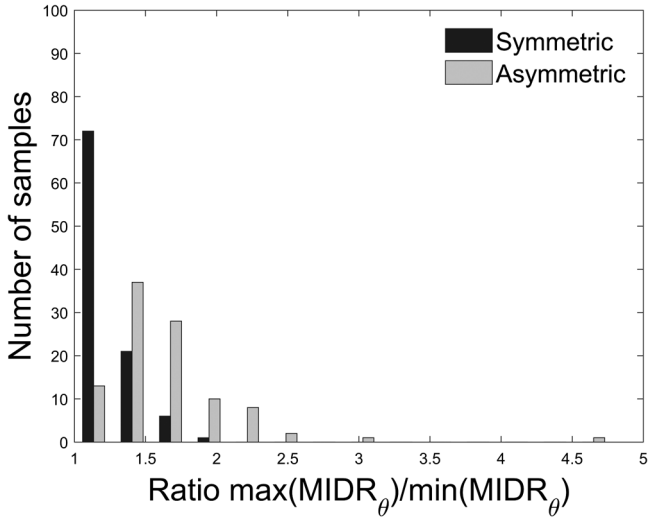

FIGURE 11 Ratios between the highest and the lowest MIDRs

(Top, Right). This figure shows that the variability between sets of IM-EDP points calculated for each incidence angle is very similar. However, there is a shift of the central values, especially in the dissimilar-axes structure. This is because the slope of the regression line in the log-log space remains practically the same, whilst the intersection point with the ordinate axis varies depending on the incidence angle (see Figure 4, bottom). This dependency increases along with the damage state under consideration. The extreme consequence of this shift can be quantified by subtracting the lowest fragility function from the highest, as depicted in Figure 12 (Bottom). From this operation, differences in probability of up to 0.04 are detected for the similar-axes building, whilst for the dissimilar-axes one they reach values in the order of 0.2. Note that this source of variability cannot be attributed to the number of records, since Figure 7 shows that the vertical intercept stabilizes from 60 records onwards.

Figure 12 also shows collapse fragility functions for the un-rotated components, which fall roughly in the middle of each population. While this finding should not be generalized to other structures and ground motion sets, it is a good indication of the statistically insignificant variation of the unharmonized set vis-à-vis consistent group-level rotations, leading to the conclusion that who argued that in the absence of any predominant orientation, a random orientation may be employed without introducing significant bias.[16,17,36]

So far, the incidence angle has been treated as uncertain, meaning that the ground motion could act in any direction, as no harmonization has been performed per individual record with respect to the incidence angle of seismic waves relative to the recording seismograph. Thus, within the realm of incidence-agnostic probabilistic assessment, any of the fragility curves presented in Figure 12 is valid to represent the IM-EDP relationship.

5.3 | Extreme fragility curves

Fragility functions presented in Figure 12 are estimated considering that seismic sources potentially affecting buildings are randomly located around the site. Extreme cases would be that the incidence angle of the ground motions always maximizes or minimizes the structural response. These curves are identified as *extreme fragility functions*, and they can be obtained when each ground motion is rotated so that the maximum responses, in terms of EDPs, are aligned. If a nominal incidence angle of 0° is assigned, and the entire group of records is rotated consistently by using increments of 1° from this orientation, the fragility curves of Figure 13 (Top) are obtained. Clearly, by aligning the maxima (and consequently the minima), the dispersion vis-à-vis Figure 12 is considerably increased. Moreover, it can be seen that the dispersion increases along with the dissimilarity of the axes of the structure. Figure 13 (Bottom) shows the differences between the highest and the lowest fragility functions. For the similar-axes structure, differences in the order of 0.35 may be reached, whilst in the dissimilar-axes case the maximum observed value is 0.5. However, such curves are only useful for establishing worst-case scenarios: *Using the maximum response when designing or assessing a structure, leads to substantially increased probabilities of exceeding specific damage states*. Thus, a scenario where one can reasonably justify rotating records to a non-arbitrary

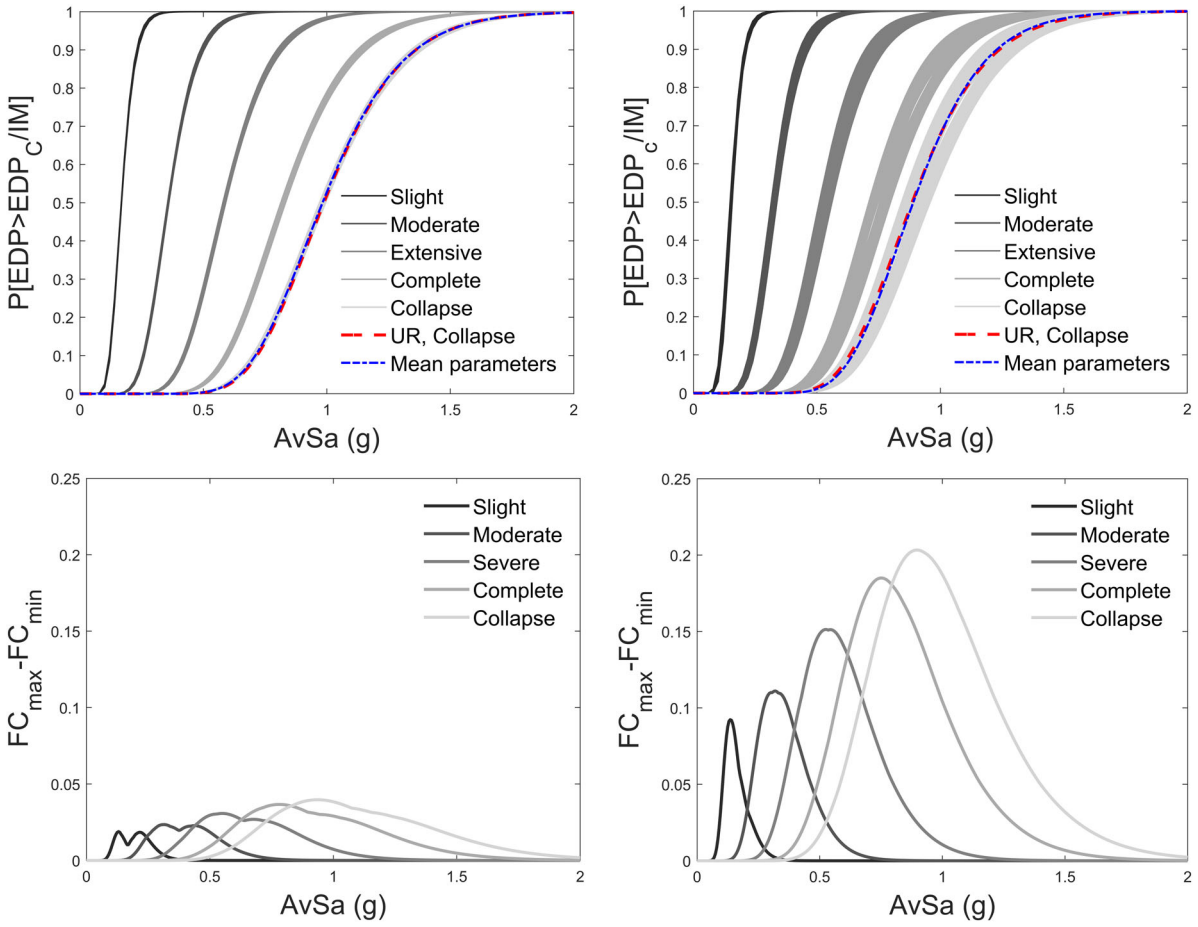

FIGURE 12 Top: Fragility functions depending on the incidence angle; similar- (Left) and dissimilar-axes (Right) structures. Bottom: Maximum differences in the conditional probabilities of being in each damage state

angle is for taking into account the actual orientation of a building with respect to the fault, which is not necessarily the worst-case scenario (see[37]).

6 | INCIDENCE-CONSISTENT FRAGILITIES

When assessing seismic risk at urban scale by simulating earthquake scenarios (i.e. by simulating a rupture and the consequent seismic waves propagation), one could take into account the azimuthal position of the structures with respect to the epicentre. In case of a fault contributing most to the hazard, the orientation of structures would play a key role in their resulting risk. That is, rather than using random incidence, one may consider adopting for any given event an incident angle that is consistent with the relative location of the site and the rupture. Similar to the multiple definitions of the rupture-to-site distance,[38] there can be many reference points on the rupture plane to define an incidence angle with respect to a building's principal axes: The epicentre, the closest point to the building site, etc. In the present case, it has been employed as reference the epicentre to define the site-to-epicentre line, so called St-Ep. The angle between a building's principal axis (or a seismograph's recording axis) and the St-Ep line is the so-called epicentre back-azimuth. In the following, consistent rotations with respect to this line are considered for estimating fragility functions.

6.1 | Axes of interest

Previous sections have shown that the horizontal response of buildings strongly depends on the incidence angle of the dynamic action. This is because the stiffness varies along with their horizontal axes. In rectangular structures, as the ones analysed in this study, the most flexible axes are parallel and orthogonal to the principal 'x' and 'y' axes (Figure 1),

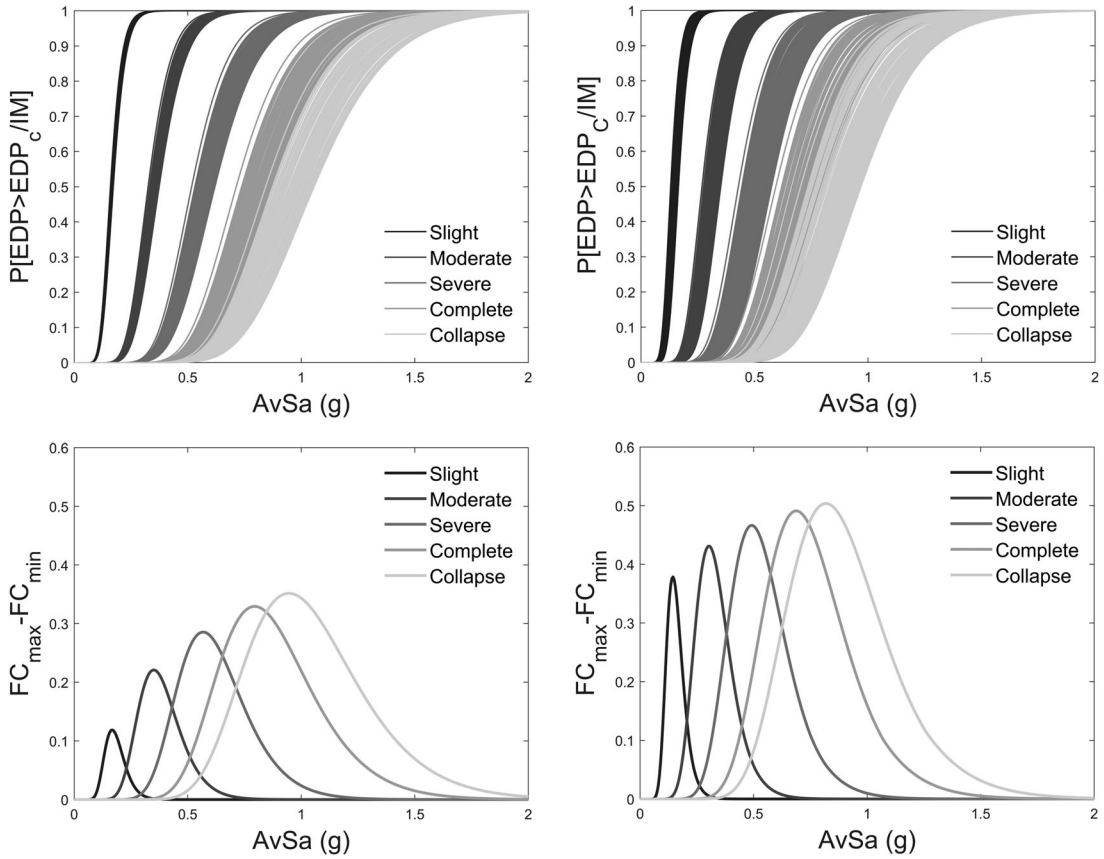

FIGURE 13 Top: Fragility functions derived so that at 0° MIDR is maximum; similar- (Left) and dissimilar-axes (Right) structures. Bottom: Maximum differences in the conditional probabilities of being in each damage state

lying at epicentre back-azimuths of a_x and a_y, respectively. A nominal "maximum-stiffness" axis back-azimuth, a_β, can be estimated with respect to the x-axis at an angle β as follows:

$$\beta = \tan^{-1}\left(\frac{k_y}{k_x}\right) \tag{5}$$

where k_y and k_x are the stiffness related to equivalent SDoF oscillators whose fundamental periods are T_y and T_x, respectively. Considering that $k_n = 4m\pi^2/T_n^2$, Eq. 5 can be rewritten as follows:

$$\beta = \tan^{-1}\left(\frac{T_x^2}{T_y^2}\right) \tag{6}$$

According to Eq. 6, the similar-axes structure has its maximum-stiffness axis at 45° with respect to the main axis, whilst the dissimilar has it at 58°, clearly drawn by the higher stiffness of the y axis (see Figure 14).

It can be claimed that by rotating the ground motions to align with the principal and the maximum-stiffness axes, i.e., at back-azimuths of a_x, a_y and a_β, one can sufficiently envelope a building's behavior under consistent rotations. The corresponding geometric alignments are presented in Figure 15 (Top) for the similar-axes (only two due to symmetry) and Figure 15 (Bottom) for the dissimilar-axes building.

6.2 | Consistent rotations, similar-axes structure

Fragility functions shown in Figure 16 (Top, left) are calculated considering the consistent rotations assigned to the similar-axes structure as well as the UR signals. When rotating the structure so that the main axes are parallel or orthogonal to

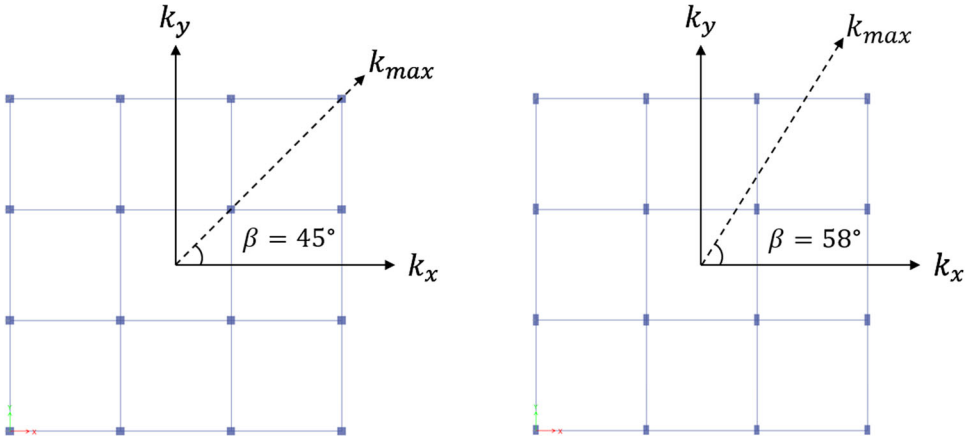

FIGURE 14 Location of the stiffest axis of the similar- and dissimilar-axes structures

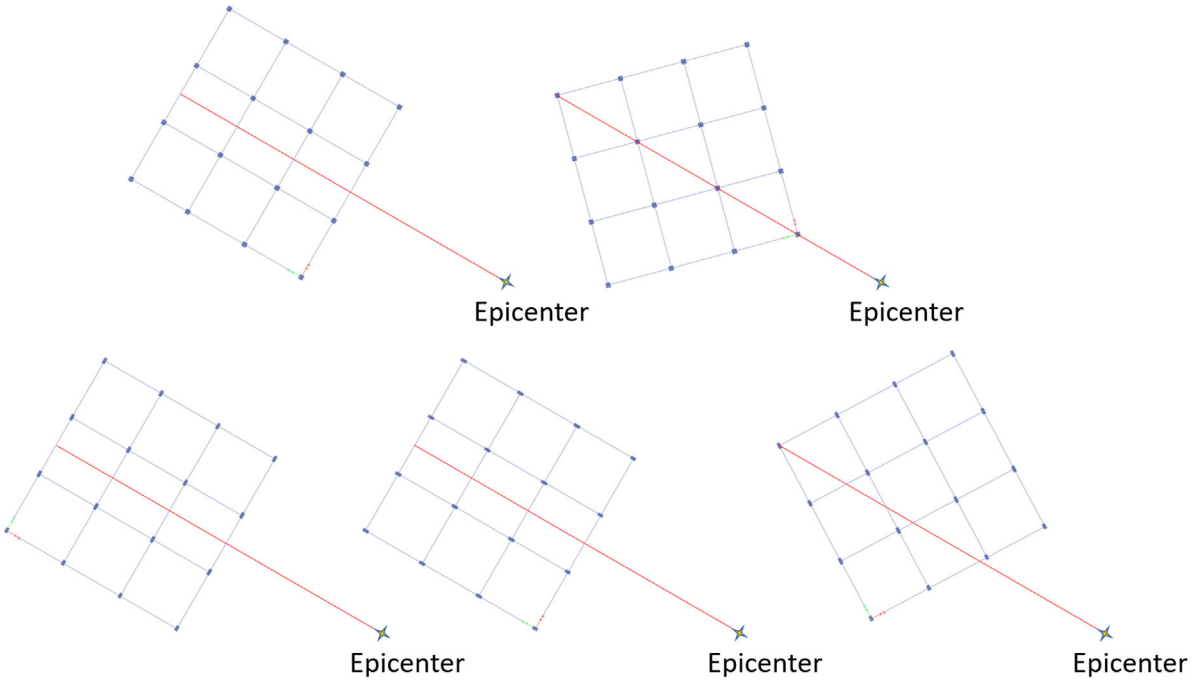

FIGURE 15 Consistent rotation for the similar- (Top) and dissimilar-axes structures (Bottom)

the St-Ep line, the resultant functions provide probabilities above the ones calculated using the UR signals. The opposite happens when rotating the main axes of the structure at 45° with respect to the St-Ep line (i.e. stiffest axis).

Fragility curves shown in Figure 16 (Top) have been obtained after considering the entire set of records (one-hundred in total). In order to analyse how the proximity to the fault influences the directionality effect, Figure 16 (Middle and bottom, left) shows fragility curves considering two subsets of fifty records classified according to the distance-to-the-hypocentre (HD) being below or above 19.65 km. Separating these records to obtain fragility functions shows that the azimuthal position of the building has more influence on the expected damage when considering the set of nearer fault records. In this case, the fragility functions related to the UR components tend to fall approximately in the middle of the curves considering the consistent rotations. For far-field records, the azimuthal position of the building seems to have little influence on the damage estimate.

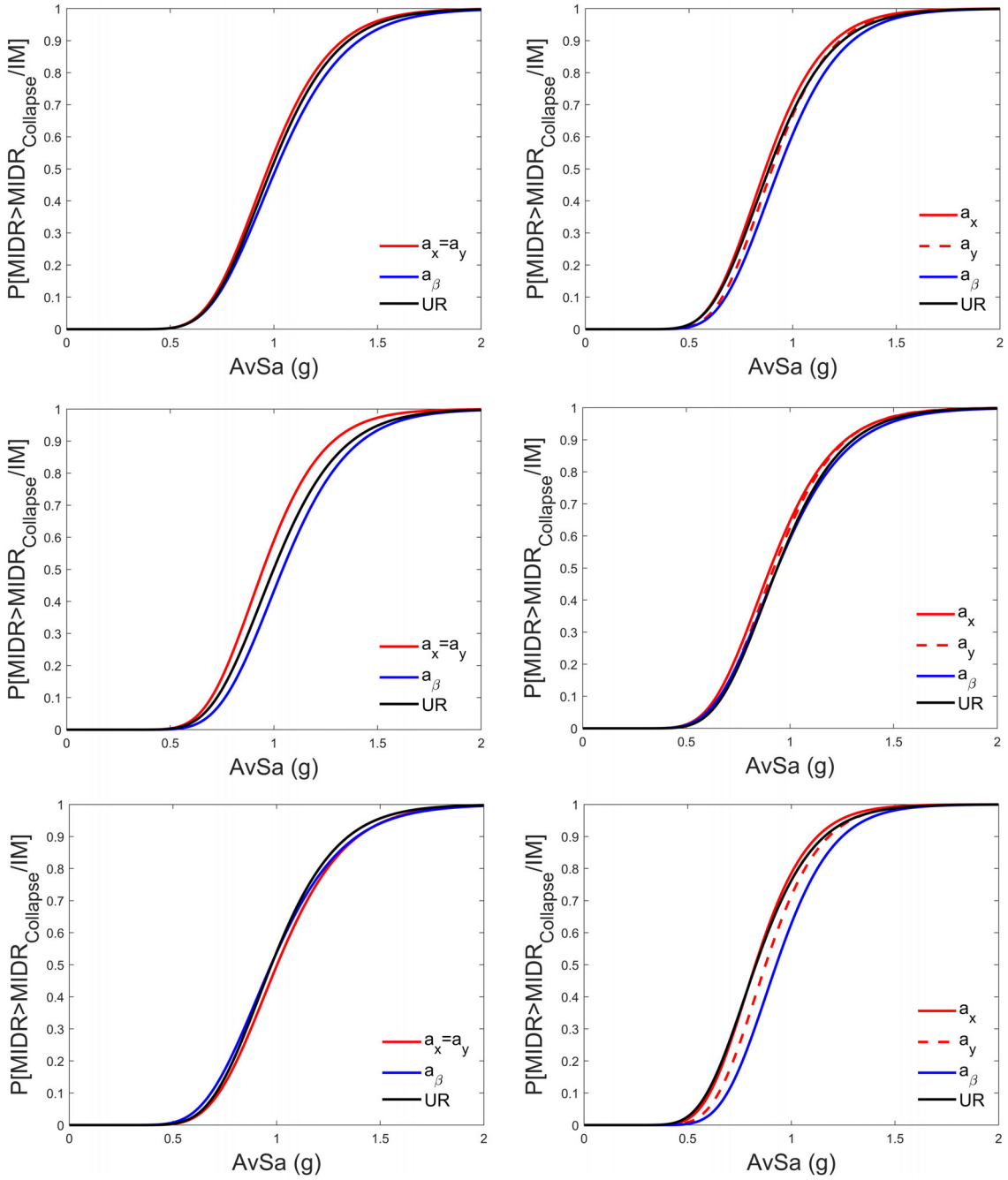

FIGURE 16 Incidence-consistent fragility curves; Top: All the records; middle: HD < 19.65 km; bottom: HD ≥19.65 km. The UR-based fragility estimated is also shown. Left: Similar-axes structure; Right: Dissimilar-axes structure

6.3 | Consistent rotations, dissimilar-axes structure

Figure 16 (Top, right) presents fragility functions for the consistent rotations proposed for the dissimilar-axes structure; the entire set of records has been used to derive these curves. As in the similar-axes case, when rotating the structures so that the x-axis is parallel to the St-Ep line, the resultant fragility function gives probabilities above the ones expected using the UR signals. In the case of rotating by a_y, the fragility function is similar to the one provided by the UR signals. For the maximum-stiffness axis, a_β, probabilities below the ones calculated with the UR signals are observed. If the distance classification is considered again, fragility functions related to a_x and a_y for nearer ground motion records provide higher probabilities of exceedance than the ones using the UR signals (Figure 16, middle, right); for the maximum stiffness axis, similar probabilities to those given by the UR signals are observed. For far-field records (Figure 16, bottom and right), the

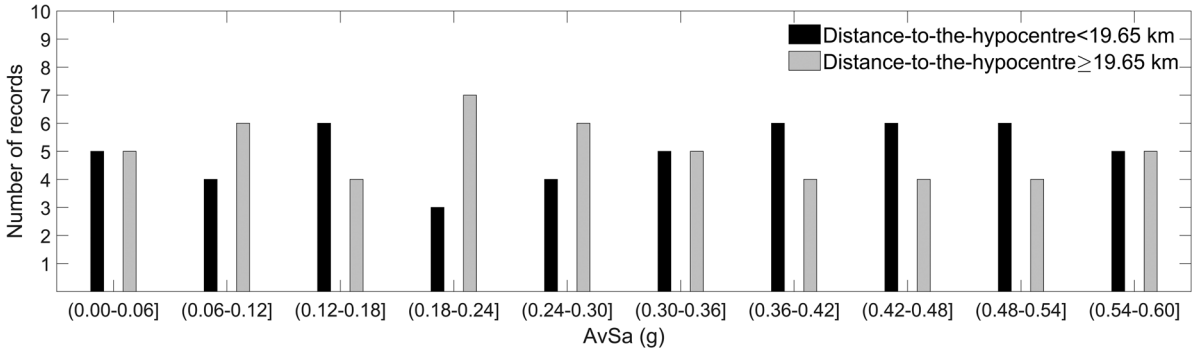

FIGURE 17 AvSa distributions for records with distance-to-the-hypocentre below and above 19.65 km

fragility curve using UR components envelopes the ones related to the consistent rotations. For both subsets of records, the condition that the fragility functions associated to the maximum stiffness axis provide lower probabilities of exceedance than the ones related to the main axes is met.

However, evidence presented in Figure 16 (middle and bottom) is limited since only 50 records have been considered to derive these fragility functions; according to Figure 7, at least 60 records are necessary to stabilize the vertical intercept, which is the variable controlling bias in fragility functions. In addition, when splitting the set of records according to HD, the sampling uniformity of the IM values may be compromised. It is because the number of records per interval is not constant (see Figure 17), as when the entire set is considered. Thus, to verify whether the trend observed in Figure 16 is not due to the limited number of records, or their IM distributions, new calculations have been carried out in the following section by guaranteeing both characteristics.

6.4 | How to include the azimuthal position of structures in seismic risk estimations?

According to the results presented above, expected seismic damage seems to depend on both the distance-to-the-hypocentre of the building and its azimuthal position. In order to account for such dependencies in seismic risk assessments, one could derive a coefficient to adjust the UR-based fragility functions due to the azimuthal position, distance-to-the-hypocentre, and axes dissimilarity of the structure. The data so far points to the fact that, by virtue of having similar variabilities, fragility functions calculated for consistent rotations can be regarded as shifted versions of the one obtained with the UR signals. Accordingly, the following correction factor can be calculated:

$$cf_{a_n} = \frac{\mathrm{IM}_{(a_n,\, MIDR_C)}}{\mathrm{IM}_{(UR,MIDR_C)}} \tag{7}$$

where $\mathrm{IM}_{(a_n,\, MIDR_C)}$ is the IM value associated with the median of the fragility function for a back-azimuth of a_n; $\mathrm{IM}_{(UR,MIDR_C)}$ is the IM value associated with the median of the fragility function for the un-rotated records. Given that the variabilities remain similar, cf_{a_n} allows shifting the UR-based fragility function depending on the azimuthal orientation of buildings with respect to the epicentre.

In addition, results presented in Figure 16 suggest that cf_{a_n} will depend on the proximity to the fault. In order to quantify this dependence, five bins are formed covering records whose distance-to-the-hypocentre are (0-10] km, (10-20] km, (20-30] km, (30-40] km and > 40 km. Two-hundred records have been selected per each bin. The bootstrap procedure[39] has been used to verify the statistical significance of cf_{a_n}. Specifically, the two-hundred records in each bin have been sampled with replacement, forming one-hundred alternate sets of two-hundred records each, in turn used to generate new fragilities and recalculate cf_{a_n}. The damage threshold to be exceeded has been collapse (see Table 2).

The error bars in Figure 18 show the 90% percentile confidence intervals for each case. It is quite clearly the norm for both structures when lower hypocentral distances are considered. The size of the effect may be on the low side, but there are several cases where its presence cannot be easily discounted, with the difference expected to grow for plan-asymmetric structures or larger dissimilarities in the two axes. For the subset of records whose distance-to-the-hypocentre is in the interval 0–10 km, cf_{a_n} tends to fall below 1 if the most flexible axis is parallel to the St-Ep line, and vice-versa if the stiffest axis is parallel to this line. Although this occurs for both structures, higher cf_{a_n} values are foreseen for the

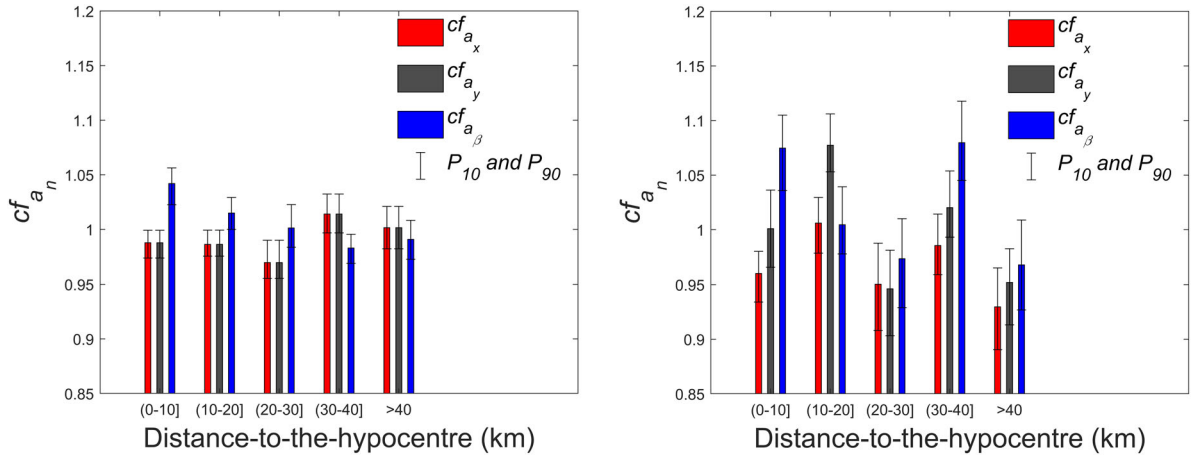

FIGURE 18 Correction factor, cf_{a_n}, for the collapse fragility function depending on the azimuthal position of the building and maximum distance-to-the-hypocentre. Left: Similar-axes building. Right: Dissimilar-axes building. P_{10} and P_{90} 10th and 90th percentiles, respectively

TABLE 3 cf_{a_n} for the subset of records in the interval 0–10 km

	Similar-axes		Dissimilar-axes		
	$\overline{cf}_{a_x=a_y}$	$\overline{cf}_{a_\beta}$	$\overline{cf}_{a_x}$	$\overline{cf}_{a_y}$	$\overline{cf}_{a_\beta}$
Slight	0.9959	1.0131	0.9900	1.0060	1.0240
Moderate	0.9912	1.0252	0.9763	1.0062	1.0483
Severe	0.9875	1.0339	0.9660	1.0017	1.0483
Complete	0.9879	1.0390	0.9625	0.9996	1.0684
Collapse	0.9835	1.0396	0.9612	0.9995	1.0734

dissimilar-axes building than for the similar-axes one. From these results, one could obtain cf_{a_n} values to adjust fragility functions derived for UR signals. Accordingly, Table 3 shows the median cf_{a_n} values for the limit-states presented in Table 2.

Note that the adjustment coefficient may be small, but, what is important is not the value itself (6-7%) but the consequence of it. That is, adjustments in the order of 6–7% produce differences in probability in the fragility functions of about 15% with respect to the un-rotated case. When one discusses random orientations of one structure relative to several seismic sources, such differences can be neglected,[16,17] yet they produce a consistent non-negligible bias for a given scenario event when considering similarly oriented structures, as often happens in historical city cores. This bias can be even higher, as it will be shown below.

6.5 | Will the fragility of other structures depend on their azimuthal position?

When considering nearer records, it has been detected that MIDR tends to increase if the main axes of two rectangular RC structures are oriented parallel or orthogonal to the St-Ep line. Also, MIDR has the tendency to decrease if the stiffest axis is parallel to this line. In order to consider this effect in seismic risk estimations, one could shift fragility functions obtained with UR components. The direction of the shifting depends on the orientation of the main axes with respect to the St-Ep line. It is of interest to verify if this tendency is expectable in other building types. However, if MDoF nonlinear models are used to analyse the behaviour of other structures, the computational time to reach similar results to those presented in previous sections would be excessive. Simplifying the structural model would diminish the computational effort allowing analysing several building models in a fraction of time. In this sense, one of the most simplified representation of a building is an SDoF system. This model has been extensively used to estimate the dynamic response of civil structures.[40–42] Based on this simplified representation, it is proposed to approximate the 3D dynamic response of a building by combining the time history response of two uncoupled linear elastic SDOF systems in orthogonal axes. To do so, the dynamic equilibrium

equation for SDoF systems in the n direction has been considered:

$$m\ddot{u}_n(t) + c\dot{u}_n(t) + ku_n(t) = -m\ddot{u}_{g,n}(t) \tag{8}$$

where $\ddot{u}_n(t)$, $\dot{u}_n(t)$ and $u_n(t)$ are the acceleration, velocity and displacement time history responses of the SDoF in the n direction, respectively; $\ddot{u}_{g,n}(t)$ is the acceleration ground motion; m, c, and k represent the mass, damping and stiffness of the system, respectively. Thus, the maximum 3D time history response of the system in terms of displacement can be estimated as follows:

$$u_{max} = max\left(\sqrt{u_x^2(t) + u_y^2(t)}\right) \tag{9}$$

From this response variable, several EDPs can be estimated to obtain cf_{a_n} points analogous to those presented in Figure 18. In order to perform these calculations, a new group of ground motion records are selected according to the procedure presented in section 3. However, this procedure demands one set of records per structure, as the period intervals for averaging the spectral acceleration change depending on the dynamic properties of the system. To avoid this, the new set of records is selected so that AvSa is estimated in a range considering the period limits of all the models under analysis. That is, ten records per interval whose AvSa in the range of 0.02–1.8 sec is between a band limited by two intensity levels. The intensity levels defining the upper and lower limits of each band range from 0.1 to 1 g at intervals of 0.1 g. The distance-to-the-hypocentre of these records is lower than ten Km. Summarizing, the following procedure is considered to obtain five-hundred cf_{a_n} points based on SDoF oscillators:

1. Generate a uniform random sample within the interval [0.2 - 1] s. This sample represents the fundamental period of an RC structure in the x direction, T_x
2. Calculate T_y as a random fraction of T_x. This fraction is obtained as a uniform random sample varying within the interval [0.75 - 1]. This way, the convention of having the most flexible axis coinciding with the x-axis is maintained
3. Estimate the angles for performing the consistent rotations according to the St-Ep line for each record
4. For each consistent rotation and for the UR components, estimate EDPs for the entire set of records
5. Calculate fragility functions for each group of points obtained in the previous step
6. Estimate cf_{a_n}
7. Repeat steps 1 to 6 until having five-hundred cf_{a_n} points

The EDP to be analysed (step 4) is the global drift experimented by the building, *GD*. This EDP is highly used in estimations of the seismic risk via CSM. It is worth noting that the MIDR of an MDoF system can be estimated from the *GD* according to the procedure presented in.[29] Herein, as the building height is unknown, *GD* is estimated by means of the following equation:

$$GD = PF_1 \frac{u_{max}}{H_{eq}} \tag{10}$$

where PF_1 is the mode participation factor[43]; H_{eq} is the equivalent height of the building which is estimated using the recognised expression stating that the fundamental period of an RC structure can be approximated as dividing its number of storeys by ten. For the sake of simplicity, PF_1 has been estimated as follows:

$$PF_1 = 1 + 0.45T_{XY} \tag{11}$$

This way, for a hypothetical 10-storey building, PF_1 will be 1.45, whilst for a 2-storey one it will be 1.09.

Figure 19 (Left) shows the relationship between T_{XY} and the shifting coefficients using *GD* as EDP. The threshold to be exceeded has been $GD_C = 0.025$. Figure 19 (Right) shows the evolution of the shifting coefficient when related to $R_{T_{XY}}$ (see equation 1).

When analysing the relationship between cf_{a_β} and T_{XY}, one could observe that there is a tendency of the data to provide a shifting to the right if the a_β axis is parallel to the St-Ep line. Several results (68.2%) meet the condition that $cf_{a_\beta} > cf_{a_x}$. Also, 40.6% of the time $cf_{a_\beta} > max(cf_{a_x}, cf_{a_y})$ and 54.6% of the time $cf_{a_y} > cf_{a_x}$. This indicates that the probability of

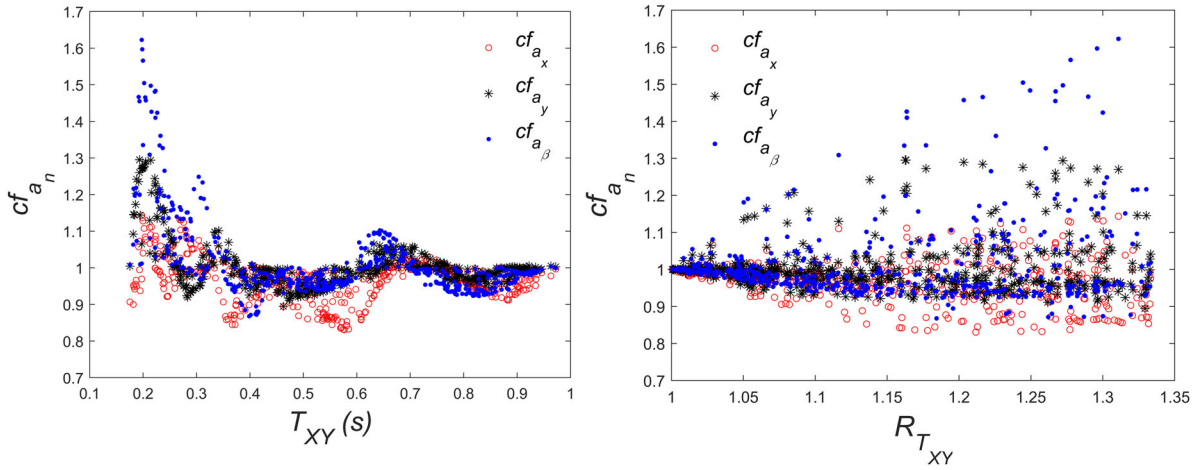

FIGURE 19 $\boldsymbol{cf_{a_n}}$ using SDoF linear models. Left: $\boldsymbol{T_{XY}}$. Right: $\boldsymbol{R_{T_{XY}}}$

exceedance GD_C tends to diminish if the stiffest axis is oriented parallel to the St-Ep line. This tendency is even more pronounced for specific T_{XY} intervals. For instance, if only data in the interval [0.175 - 0.7] s are analysed, 83.2% of the time $cf_{a_\beta} > cf_{a_x}$, 59% of the time $cf_{a_\beta} > max(cf_{a_x}, cf_{a_y})$ and 74.9% of the time $cf_{a_y} > cf_{a_x}$. Regarding $R_{T_{XY}}$, the higher this variable, the higher the dispersion of the data. This implies that higher shifts of the fragility functions are expected for structures exhibiting dissimilarities of the horizontal stiffness. In general, no shifting is foreseen (In terms of statistical significance) if buildings are oriented parallel to axis a_y.

Note that both EDPs, *GD* and MIDR, are highly correlated, as shown in Vargas et al 2019. They have also proven that this correlation increases if the average response of several SDoF oscillators is used instead of that related to the fundamental period of the structure; thus, the estimation of the cf_{a_n} points would be probably more accurate. Note also that if $R_{T_{XY}}$ approaches 1, cf_{a_n} tends to 1. This is because the resultant of orthogonal forces in similar-axes linear systems is insensitive to variation of the incidence angle. Since low shifts are expected for similar-axes buildings (see Figure 18, left) and nonlinearities may increase cf_{a_n} values, further analysis should be performed using non-linear MDOF models to better parameterize the relationship between cf_{a_n} and $R_{T_{XY}}$. Anyhow, results presented in Figure 19 confirm the dependency of the horizontal response on the azimuthal position of the analysed systems when considering near-fault records. Overall, seeing the similar trends of the (limited) MDOF and (extensive) SDOF results, one may expect similar findings for other 3D MDOF structures, at least for damage states that are predicted well by the first translational mode in each direction. This dependency may vary depending on the range of periods analysed, as indicated in Figure 19. Therefore, the applicability of the procedure should be limited, for the time being, to EDPs related to the global deformation of the structure, i.e., the MIDR, or the GD. Further research should be oriented to verify the methodology proposed herein when considering new EDPs or IMs.

7 | CONCLUSIONS

This study has addressed the influence of the directionality effect on seismic risk estimations. To do so, the fragility of two RC structures has been analysed via cloud analysis.[22] The main difference between the structures is the dissimilarity level of the horizontal stiffness with respect to the main axes; one of them have similar-axes whilst the other has a certain level of dissimilarity. Although both structures have the ability to withstand similar gravitational loads, it has been observed that the dissimilar-axes building tends to be more vulnerable to suffer seismic damage than the similar-axes one. This conclusion has been reached after deriving fragility functions for both structures using the same set of ground motion records. It has also been observed that the dissimilarity level tends to increase the variability of the horizontal response of structures if the directionality effect is taken into consideration. For instance, the ratio between the highest and the lowest MIDR, when varying the incidence angle, increases along with the dissimilarity level of the structure (see Figure 11).

The variability introduced by the incidence angle on the fragility functions has been quantified. Two approaches have been considered to take it into account. In the first one, the incidence angle has been assumed as epistemic uncertainty.

This is compatible with probabilistic seismic risk estimations in which one would expect ground motions coming from any direction. Results showed that even in this case, the rotation of the horizontal components of the records may introduce some added variability, but low bias (almost non-existent for similar-axes structures, see Figure 12, bottom and left). In the second approach, consistent rotations are proposed to consider the actual orientation of buildings with respect to the epicentre. It has been shown how the proximity to the hypocentre may affect the expected fragility of the structures when performing these consistent rotations, an effect that is separate from any directivity or other near-source effects.

In the case of the consistent rotations, a correction factor, cf_{a_n}, to modify fragility functions derived with UR signals has been obtained. This coefficient augments or reduces the probability of exceeding certain damage states, depending on whether the most flexible axis of the structure or the stiffest one is aligned with the St-Ep line. This indicates that urban environments may be more prone to damage in a specific orientation, especially if the street layout is consistent with a regular grid, as is the case in various cities around the world. For single structures, their azimuthal orientation can be used to modify fragility functions so that the probability of exceeding certain damage threshold can be recalculated in an event-to-event analysis. In this way, the expected fragility of each structure will also depend on the location of the rupture with respect to the azimuthal position of the structure. To do so, it will be necessary to identify likely values of the horizontal stiffness of structures belonging to actual urban environments. However, the number of structures in large cities is high, which requires the development of an automatic procedure to identify this characteristic. This could be achieved using pattern recognition tools aimed at analysing aerial images of urban environments.

Note that using the UR components as reference to calculate the correction factor has provided satisfactory results (see Figure 18 and Figure 19). However, the SDOF results show that in some cases this approach is not appropriated since the mean value related to the UR fragility functions may not fall in the middle of the population. This issue may be addressed by calculating cf_{a_n} with respect to a midpoint between fragility functions related to a_x and a_β (Representing x and β the most flexible and stiffest axes, respectively).

It is also important to clarify that the influence of the azimuthal position of the structures is not important for all the structures or sites, or combination of the two, there are indeed many cases in which this is not even a problem. This could be for example the case of multiple sources all around the city, where no specific orientation beneficial or detrimental, but in case of a fault contributing most to the hazard, the orientation of structures built according to a consistent grid would play a role in their resulting risk.

The IM to perform the calculations presented in this research has been AvSa. It will be of interest to analyse the sensitivity of the shifting coefficient if other IMs more efficient than AvSa are considered. Energy-based as well as velocity-based IMs are ideal candidates to perform this analysis.[44–46] Other consistent rotations should also be explored to verify if any of them allow the effect of directionality to be captured most accurately.

Finally, as has been demonstrated in this article, seismic risk assessment methods may be enhanced in terms of efficiency if the location of the faults, the azimuthal position of buildings along with the direction of their most flexible and stiffest axes are known and accounted for on an event-per-event basis in the estimation of losses and risk, removing the pertinent uncertainties. However, since only two nonlinear MDOF models have been used along with uncoupled elastic SDOF responses, it is very difficult to establish the range of applicability of the results presented. Further research is required to confirm whether the results presented exhibit the same trend if other structural typologies, plan shapes, materials, or different design levels are analysed. For structures with significant higher-mode influence, preliminary results point to a reduced sensitivity of MIDR to consistent incident angle rotations; the opposite happens for more rigid structures. Still, this remains to be verified in the future.

Results presented in this article meet the principles of fair data.[47] Thus, potential users could find, access, interoperate and reuse data presented herein. Text files containing the main results as well a document describing the data arrangement can be downloaded from the following website: http://kairoseq.upc.edu.

ACKNOWLEDGEMENTS

Yeudy F. Vargas-Alzate has been granted an Individual Fellowship (IF) in the research grant program of the Marie Sklodowska-Curie Actions (MSCA), European Union/European (H2020-MSCA-IF-2017) No 799553. This author is deeply grateful to this institution.

DATA AVAILABILITY STATEMENT

The data that support the findings of this study are openly available in http://kairoseq.upc.edu

ORCID

Yeudy Felipe Vargas-Alzate https://orcid.org/0000-0001-7049-071X
Dimitrios Vamvatsikos https://orcid.org/0000-0002-4016-5040
Lluis Gonzaga Pujades https://orcid.org/0000-0002-2619-0805

REFERENCES

1. Federal Emergency Management Agency. *FEMA P-58: Seismic performance assessment of buildings*. Washington, DC: Federal Emergency Management Agency; 2012
2. Basset-Salom L, Guardiola-Víllora A. Seismic performance of masonry residential buildings in Lorca's city centre, after the 11th May 2011 earthquake. *Bull Earthq Eng*. 2014;12:2027-2048.
3. Roeslin S, Ma QTM, García HJ. Damage assessment on buildings following the 19th September 2017 Puebla, Mexico earthquake. *Front Built Environ*. 2018;4:72
4. Bradley BA, Baker JW. Ground motion directionality in the 2010–2011 Canterbury earthquakes. *Earthq Eng Struct Dyn*. 2015;44(3):371-384.
5. Spudich P, Chiou BSJ, Graves R, Collins N, Somerville P. A formulation of directivity for earthquake sources using isochrone theory. *U.S. Geol Surv Open-File Rept*. 2004;54;2004-1268.
6. Boore M, Watson-Lamprey J, Abrahamson N. Orientation-independent measures of ground motion. *Bull Seismol Soc Am*. 2006;96(4A):1502-1511.
7. López OA, Torres R. The critical angle of seismic incidence and the maximum structural response. *Earthqe Eng Struct Dyn*. 1997;26:881-894.
8. López OA, Chopra AK, Hernandez JJ. Critical response of structures to multicomponent earthquake excitation. *Earthq Eng Struct Dyn*. 2000;29:1759-1778.
9. Rigato AB, Medina RA. Influence of angle of incidence on seismic demands for inelastic single-storey structures subjected to bi-directional ground motions. *Eng Struct*. 2007;29:2593-2601.
10. Reyes JC, Kalkan E. Significance of rotating ground motions on behavior of symmetric-and asymmetric-plan structures: part I. Single-story structures. *Earthq Spectra*. 2015;31:1591-1612.
11. Kalkan E, Reyes JC. Significance of rotating ground motions on behavior of symmetric-and asymmetric-plan structures: part II. Multi-story structures. *Earthq Spectra*. 2015;31:1613-1628.
12. Lagaros ND. Multicomponent incremental dynamic analysis considering variable incident angle. *Struct Infrastruct Eng*. 2010;6: 77-94.
13. Torbol M, Shinozuka M. The directionality effect in the seismic risk assessment of highway networks. *Struct Infrastruct Eng*. 2012;10:175-188.
14. Vargas-Alzate YF, Pujades LG, Barbat AH, Diaz-Alvarado SA, Hidalgo-Leiva DA. Probabilistic seismic damage assessment of reinforced concrete buildings considering directionality effects. *Struct Infrastruct Eng*. 2018;14(6):817-829.
15. Pinzón LA, Pujades LG, Diaz-Alvarado SA, Alva RE. Do directionality effects influence expected damage? A case study of the 2017 Central Mexico earthquake. *Bull Seismol Soc Am*. 2018;108(5A):2543-2555.
16. Giannopoulos D, Vamvatsikos D. Ground motion records for seismic performance assessment: to rotate or not to rotate? *Earthq Eng Struct Dyn*. 2018;47(12):2410-2425.
17. Skoulidou D, Romão X, Franchin P. How is collapse risk of RC buildings affected by the angle of seismic incidence? *Earthq Eng Struct Dyn*. 2019;48(14):1575-1594.
18. Otani S. Inelastic analysis of RC frame structures. *J Struct Div ASCE*. 1974;100:1433-1449.
19. Carr AJ. *Ruaumoko-Inelastic Dynamic Analysis Program*. Christchurch, New Zealand: Department of Civil Engineering, University of Canterbury; 2000.
20. Haselton CB, Whittaker AS, Hortacsu A, Baker JW, Bray J, Grant DN. Selecting and Scaling Earthquake Ground Motions for Performing Response-History Analyses. Proceedings of the 15th World Conference on Earthquake Engineering, Lisboa, Portugal; 2012.
21. Luco N, Bazzurro P. Does amplitude scaling of ground motion records result in biased nonlinear structural drift responses? *Earthq Eng Struct Dyn*. 2007;36(13):1813-1835.
22. Jalayer F, De Risi R, Manfredi G. Bayesian Cloud Analysis: efficient structural fragility assessment using linear regression. *Bull Earthq Eng*. 2015;13:1183-1203.
23. Luzi L, Puglia R, Russo E, and ORFEUS WG5. Engineering Strong Motion Database, version 1.0. Instituto Nazionale di Geofisica e Vulcanologia, Observatories & Research Facilities for European Seismology. 2016 https://doi.org/10.13127/ESM
24. Luco N, Cornell CA. Structure-specific scalar intensity measure for near-source and ordinary earthquake motions. *Earthq Spectra*. 2007;23:357-392.
25. Lin T, Haselton CB, Baker JW. Conditional spectrum-based ground motion selection. Part I: hazard consistency for risk-based assessments. *Earthq Eng Struct Dyn*. 2013;42(12):1847-1865.
26. Eads L, Miranda E, Lignos DG. Average spectral acceleration as an intensity measure for collapse risk assessment. *Earthq Eng Struct Dyn*. 2015;44(12):2057-2073.
27. Kazantzi AK, Vamvatsikos D. Intensity measure selection for vulnerability studies of building classes. *Earthq Eng Struct Dyn*. 2015;44(15):2677-2694.
28. Kohrangi M, Bazzurro P, Vamvatsikos D, Spillatura A. Conditional spectrum-based ground motion record selection using average spectral acceleration. *Earthq Eng Struct Dyn*. 2017;46(10):1667-1685.

29. Vargas-Alzate YF, Pujades LG, González-Drigo JR, Alva RE, Pinzón LA. On the equal displacement aproximation for mid-rise reinforced concrete buildings. Computational Methods in Structural Dynamics and Earthquake Engineering. Crete, Greece, 24–26 June 2019; 2019
30. Jalayer F, Cornell CA. Alternative nonlinear demand estimation methods for probability-based seismic assessments. *Earthq Eng Struct Dyn*. 2009;38(8):951-972.
31. Bakalis K, Vamvatsikos D. Seismic fragility functions via nonlinear dynamic methods. *ASCE J Struct Eng*. 2018:144. ASCE.
32. Vargas-Alzate YF, Pujades LG, Barbat AH, Hurtado JE. An efficient methodology to estimate probabilistic seismic damage curves. *J Struct Eng*. 2019:145. ASCE.
33. Park Y, Ang AH-S. Mechanistic seismic damage model for reinforced concrete. *J Struct Eng ASCE*. 1985;111:722-739.
34. Vargas-Alzate YF, Lantada N, González-Drigo R, Pujades LG. Seismic risk assessment using stochastic nonlinear models. *Sustainability*. 2020;12:1308.
35. Aschheim M, Hernandez-Montes E, Vamvatsikos D. *Design of Reinforced Concrete Buildings for Seismic Performance: Practical Deterministic and Probabilistic Approaches Protection of Built Environment against Earthquakes*. CRC Press; 2019.
36. Beyer K, Bommer JJ. Selection and scaling of real accelerograms for bi-directional loading: a review of current practice and code provisions. *J Earthq Eng*. 2007;11(supp1):13-45.
37. Stewart JP, Abrahamson NA, Atkinson GM, et al. Representation of bidirectional ground motions for design spectra in building codes. *Earthq Spectra*. 2011;27(3):927-937.
38. Kramer SL. *Geotechnical Earthquake Engineering. Prentice-Hall Civil Engineering and Engineering Mechanics Series*. Prentice Hall: Upper Saddle River, NJ; 653; 1996.
39. Efron B, Tibshirani RJ. *An Introduction to the Bootstrap*. CRC press; 1994.
40. Dolšek M. Simplified method for seismic risk assessment of buildings with consideration of aleatory and epistemic uncertainty. *Struct Infrastruct Eng*. 2012;8(10):939-953.
41. Villar-Vega M, Silva V, Crowley H, et al. Development of a fragility model for the residential building stock in South America. *Earthq Spectra*. 2017;33(2):581-604.
42. Martins L, Silva V. Development of a fragility and vulnerability model for global seismic risk analyses. *Bull Earthquake Eng*. 2020.
43. Applied Technology Council. ATC-40 seismic evaluation and retrofit of concrete buildings; Applied technology council: redwood City, CA, USA; 1996.
44. Akiyama H. *Earthquake-Resistant Limit-State Design for Buildings*. University of Tokyo Press; 1985.
45. Bertero VV, Uang CH. Issues and future directions in the use of an energy approach for seismic-resistant design of structures. 1992. Edited by Fajfar P. and Krawinkler H. Elsevier.
46. Vargas-Alzate YF, Hurtado JE. Efficiency of intensity measures considering near-and far-fault ground motion records. *Geosciences*. 2021;11(6):234.
47. Wilkinson MD, Dumontier M, Aalbersberg IJ, Appleton G, The FAIR Guiding Principles for scientific data management and stewardship. *Scientific Data*. 2016;3:160018. https://doi.org/10.1038/sdata.2016.18

How to cite this article: Vargas-Alzate YF, Silva V, Vamvatsikos D, Pujades LG. A simplified approach for including the incidence angle effect in seismic risk assessment. *Earthquake Engng Struct Dyn*. 2022;51:191–212. https://doi.org/10.1002/eqe.3562